POLITYKA ENERGETYCZNA – ENERGY POLICY JOURNAL

2026 ✦ Volume 29 ✦ Issue 2 ✦ 33–58

DOI: 10.33223/epj/211852

Mustafa Naozad Taifor[1], Ali Azeez Ali[2], Furqan Haider Mohammed Ali[3], Adnan M. Hussein[4], Hussein Hayder Mohammed Ali[5], Mohammed Yashar Omar[6]

Numerical modeling of a hydrocyclone for the separation of oil residues in offshore installations

Abstract: This study numerically investigates oil–water separation in a hydrocyclone using the Hsieh design, selected for its manufacturability and proven experimental database. Computational Fluid Dynamics (CFD) simulations were conducted in ANSYS Fluent 16.1 employing an Eulerian–Lagrangian framework, where the water phase was resolved with the Reynolds Stress Model (RSM) and oil droplets were tracked through the Discrete Phase Model (DPM) under one-way coupling. A mesh independence study confirmed solution stability at 3.16 million cells, and residual convergence was achieved after approximately 1600 iterations, ensuring accurate predictions of velocity, pressure, and air core formation. The numerical results successfully reproduced the characteristic double-vortex flow, axial velocity reversal, and negative static pressure region

✉ Corresponding Author: Mustafa Naozad Taifor; e-mail: mustafanaozad@ntu.edu.iq

[1] Northern Technical University, Renewable Energy Research Center-Kirkuk, Iraq; ORCID iD: 0000-0001-7146-1160; e-mail: mustafanaozad@ntu.edu.iq

[2] Imam Ja'afar Al-Sadiq University, Iraq; ORCID iD: 0009-0005-7654-6389; e-mail: ali.azez@ijsu.edu.iq

[3] Kirkuk Technical Engineering College, Northern Technical University, Iraq; ORCID iD: 0009-0004-5491-3224; e-mail: furqan.haider.m.ali@ntu.edu.iq

[4] Northern Technical University, Kirkuk Technical Engineering College, Iraq; ORCID iD: 0000-0001-6689-5423; e-mail: dradnan_hwj@ntu.edu.iq

[5] Kirkuk Technical Engineering College, Northern Technical University, Iraq; ORCID iD: 0000-0003-4264-400X; e-mail: hussein_kahia@ntu.edu.iq

[6] University of Kirkuk, Iraq; ORCID iD: 0000-0001-9531-2661; e-mail: mohammedyashar6@gmail.com

© 2026. The Author(s). This is an open-access article distributed under the terms of the Creative Commons Attribution-ShareAlike International License (CC BY-SA 4.0, http://creativecommons.org/licenses/by-sa/4.0/), which permits use, distribution, and reproduction in any medium, provided that the Article is properly cited.

responsible for air core development, showing strong agreement with published experimental data. Particle tracking demonstrated that separation efficiency strongly depends on droplet size, increasing from approximately 80% for fine droplets (1–5 μm) to a maximum of nearly 90% for larger droplets (≥75 μm), resulting in an overall efficiency close to 90%. However, a fraction of water was entrained in the overflow, revealing design limitations that could be mitigated by modifying the vortex finder or underflow geometries. The validated model provides a robust framework for optimizing hydrocyclone geometry and operating conditions, contributing to enhanced oil–water separation efficiency, reduced water discharge, and improved environmental compliance in offshore production systems.

Keywords: hydrocyclone separator, oil–water separation, Reynolds Stress Model (RSM), Hsieh model, centrifugal sedimentation

List of symbols

- ρ – density [Kg/m^3]
- P – pressure [Pa]
- g – acceleration of gravity [m/sec^2]
- μ – viscosity [Pa·sec]
- V – velocity [m/sec]
- L – length [m]
- Re – Reynolds number [–]
- D – diameter [m]

List of abbreviations

- RSM – Reynolds Stress Model
- LES – Large-Eddy Simulation
- SIMPLE – Semi-Implicit Method for Pressure-Linked Equations
- DPM – Discrete Phase Model
- PIV – Particle Image Velocimetry
- CFD – Computational Fluid Dynamics
- 3D – Three Dimensional

Introduction

Hydrocyclones are considered one of the leading and widely used devices for separating solids from liquids and for separating insoluble liquids from each other (Liu et al. 2015). These devices are characterized by the absence of moving devices and the ease of their design and operation. They depend on converting the static pressure energy of the fluid into kinetic energy to provide the driving force for the separation process, as in Figure 1.

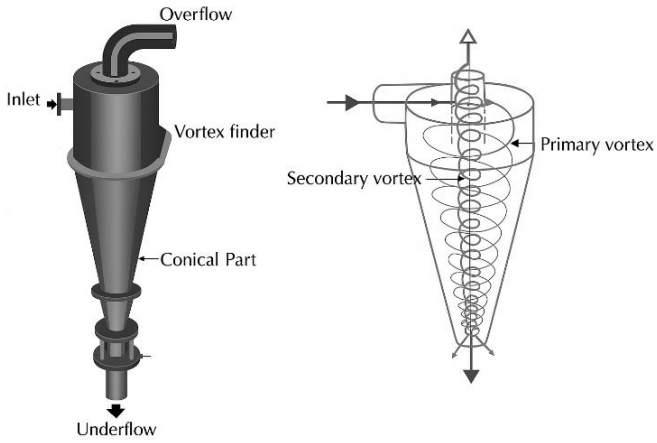

Fig. 1. Working principle of hydrocyclone

Rys. 1. Zasada działania hydrocyklonu

The working principle of these devices is based mainly on centrifugal sedimentation, which occurs due to fluid movement resulting from rotational motion. In this process, particles in the fluid are subjected to centrifugal forces that cause them to separate from the fluid. Unlike other devices that rely on the same principle, hydrocyclones do not contain any moving parts because the fluid rotational movement is acquired due to the tangential feeding of the fluid to the core of the device, which makes their use more widespread as they require low installation and maintenance costs and are easy to operate (Hsu et al. 2011; Collins 2016).

Hydrocyclones are used to separate liquids from each other or to separate liquids from solid objects suspended in them due to the density difference between the liquid and the different objects to be separated in these devices (Sorsamäki and Nappa 2015). As a result of the spiral motion that the liquid acquires when it tangentially enters the device, the particles or materials with the highest density are thrown towards the wall of the device and then drawn into the underflow current. In contrast, the movement of the lighter particles continues with the overflow current, thus forming a free vortex (the external one called the primary vortex). Another forced one (the internal one called the secondary vortex) (Varaksin and Ryzhkov 2022; Hall 1961).

Analysis of the flow in the outer core shows that the outer vortex is a free vortex in which the tangential velocity is inversely proportional to the radius. In contrast, the inner vortex is a forced vortex in which the tangential velocity increases with the increase in the radius of the flow, as shown in Figure 1.

The most crucial aspect to consider when studying flow within a hydrocyclone is the patterns of this flow, represented by the flow field composed of the three velocity components (tangential, axial, and radial), and the pressure distribution field (static and dynamic). These patterns have been studied by many researchers (Németh and Verdes 2011; Barrak et al. 2022). The basic flow patterns in the standard design of the hydrocyclone can be summarized as a vortex within a vortex, where the flow enters tangentially into the cyclone and moves in the outer area in contact with the wall in a downward rotational motion, forming the outer vortex (Ghodrat 2014). This vortex continues until reaching the bottom of the device. However, the presence of the upper central outlet and the inability of the fluid, under the conditions of regular feeding and pressure, to leave the bottom of the device, leads to the formation of a radial motion of the fluid particles moving in the outer underflow path towards the heart of the cyclone. The amount of movement of this radial motion increases as the outlet of the cone opening at the bottom of the device narrows (Long et al. 2021). Finally, the flow is forced to reverse the direction of its axial velocity, forming an upward flow in an internal vortex that moves and rotates in the same direction as the external vortex (Sarpkaya and Garrison 1963).

Three-dimensional numerical modeling using computational fluid mechanics techniques was performed by Safa Raziyeh et al. (2014) on two unique designs of hydrocyclone separators to improve the operating conditions of the cyclones and their separation efficiency. The results of this research showed that increasing the concentration of the solid phase at the inlet of the device reduces the separation efficiency while increasing the water separation rate and improving the pressure drop. The study also showed that the inlet speed into the device has a significant effect on the separation process (Safa and Goharrizi 2014). A 3D model of a hydrocyclone was performed by Xu et al. (2013) to determine the velocity field within it using the RSM turbulence model. This study presented the tangential and axial velocity profiles within the device at different heights, demonstrating an acceptable agreement with the laboratory data. Amini et al. (2012) performed a numerical modeling of a hydrocyclone to study the separation of oil pockets from water using the Eulerian and Lagrangian descriptions of the flow. This model observed that there is no mutual influence between the droplets. The comparison with the experimental results showed agreement between this model and the experimental results regarding the separation yield.

Three turbulence patterns of flow within a hydrocyclone (the same design adopted in the study for experimental comparison) were studied by Delgadillo and Rajamani (2005) using RSM and LES, and these three patterns were compared with the experimental results obtained from the proposed design. The study demonstrated that the LES model outperformed the previous two models. Motin and Bénard (2017) modeled a set of vortex chamber designs and their effect on the separation yield was directly studied after verifying the basic flow field. The study demonstrated that modifying the walls of the conical part chamber from straight to curved plays a significant role in enhancing the separation process. Thiemsakul

et al. (2024) conducted a CFD study to optimize hydrocyclone geometry for the separation of microplastics from water, systematically varying dimensional ratios and inlet design, and applying statistical analysis (ANOVA) to determine the most influential parameters. Their optimized configuration achieved 76% microplastics recovery, a 52% water split, and a pressure drop of 82,340 Pa, highlighting the trade-off between improved recovery and higher energy consumption.

Karimi et al. (2012) studied experimentally the Hsieh design to model the appearance of the air core within the cyclone, where the effect of the modeling methodology on predicting this core was examined, and the impact of changing the feed flow on the diameter of this core was also studied. The effect of changing some parameters on the performance of the hydrocyclone was studied by Murthy and Bhaskar (2012). They found that reducing the lower outlet opening caused an increase in the pressure drop, thereby decreasing the separation efficiency. Additionally, the tangential velocity component increased, thereby enhancing the separation efficiency. The aim of this study is to simulate the flow and separation processes, validate the results against experimental data, and evaluate the separation efficiency. The ultimate goal is to improve oil–water separation performance and address issues like unwanted water discharge in the overflow stream through possible design or operational modifications.

1. Mathematical analysis

The physical model encompasses the differential equations governing the flow, which involves analyzing and studying the flow field within the separator and the mechanisms of energy transfer within it (Nowakowski and Doby 2008).

1.1. Motion equations

The motion of a fluid is described by a system of differential equations derived from the conservation laws. For an incompressible Newtonian fluid, these consist of the continuity equation (mass conservation) and the three Navier–Stokes momentum equations, giving a total of four governing equations. For compressible flows or when thermal effects are considered, the energy equation is also required, depending on the working fluid and operating conditions (Temam 2024).

1.2. Continuity equation

The continuity equation expresses the principle of conservation of mass and states that the time rate of change of the mass of the control volume over a time interval is equal to the difference between the rate of mass entering and exiting it. The relationship mathematically formulates it, as shown in Equation (1) (Craik 2013; Thiemsakul et al. 2024):

$$\frac{\partial \rho}{\partial t}+\frac{\partial(\rho u)}{\partial x}+\frac{\partial(\rho v)}{\partial y}+\frac{\partial(\rho w)}{\partial z}=0 \tag{1}$$

where:

ρ – density,

u, v, w – components of the velocity in the x, y, and z directions, respectively.

Or in its compact form, as shown in Equation (2):

$$\frac{\partial \rho}{\partial t}+\vec{\nabla}.\left(\rho \vec{V}\right)=0 \tag{2}$$

1.3. Momentum equations

It represents the mathematical expression of Newton's second law, which states that when the momentum of a fluid (i.e., layers or particles of the fluid) changes, it means that a force is acting upon it (Ali et al. 2024; Szwarc et al. 2025). These Equations (3, 4, and 5) are given as follows:

Momentum equation on the x-axis:

$$\rho\left(\frac{\partial u}{\partial t}+u\frac{\partial u}{\partial x}+v\frac{\partial u}{\partial y}+w\frac{\partial u}{\partial z}\right)=-\frac{\partial p}{\partial x}+\rho g_x+\mu\left(\frac{\partial^2 u}{\partial x^2}+\frac{\partial^2 u}{\partial y^2}+\frac{\partial^2 u}{\partial z^2}\right) \tag{3}$$

Momentum equation on the y-axis:

$$\rho\left(\frac{\partial v}{\partial t}+u\frac{\partial v}{\partial x}+v\frac{\partial v}{\partial y}+w\frac{\partial v}{\partial z}\right)=-\frac{\partial p}{\partial y}+\rho g_y+\mu\left(\frac{\partial^2 v}{\partial x^2}+\frac{\partial^2 v}{\partial y^2}+\frac{\partial^2 v}{\partial z^2}\right) \tag{4}$$

Momentum equation on the z-axis:

$$\rho\left(\frac{\partial w}{\partial t}+u\frac{\partial w}{\partial x}+v\frac{\partial w}{\partial y}+w\frac{\partial w}{\partial z}\right)=-\frac{\partial p}{\partial z}+\rho g_z+\mu\left(\frac{\partial^2 w}{\partial x^2}+\frac{\partial^2 w}{\partial y^2}+\frac{\partial^2 w}{\partial z^2}\right) \tag{5}$$

where:

P – represents pressure,
g – represents the acceleration of gravity,
μ – represents viscosity.

1.4. Turbulence equations

Turbulence is defined as a random and chaotic fluctuation movement of molecules, where the speed and pressure components at any point in the flow suffer continuous changes over time. The cause of this turbulence is attributed to the presence of a source of change in the flow that leads to the formation of a turbulent signal transmitted throughout the entire flow. The flow is classified into: turbulent and laminar according to the Reynolds number criterion ($RE = \rho VL/\mu$), where L is a characteristic length, and V is a characteristic velocity. At a high Reynolds number, the flow is classified as turbulent, while at relatively low Reynolds numbers, it is classified as laminar (Ali et al. 2023).

1.5. CAD Model

The Hsieh model of hydrocyclones is chosen due to its simplicity, ease of manufacture, and the availability of a set of experimental reference studies. It can be used later in the process of verifying the numerical results obtained. The dimensions of this model are shown in Figure 2 and Table 1:

Table 1. Dimensions of Hsieh Hydrocyclone

Tabela 1. Wymiary hydrocyklonu Hsieha

D_{in}	D_{under}	D_{over}	L_1	L_2	L_3	L_4	D = 75 mm
25 mm	12 mm	25 mm	25 mm	186 mm	25 mm	50 mm	

1.5.1. Gridding process

In the current research, the geometric model was meshed using Ansys software, where the meshing was performed using tetrahedral cells, resulting in a total of 3,160,000 cells, as shown in Figure 3. The tangential velocity was chosen at a height of 0.226 m above the cyclone, and its average value was determined based on the Area-Weighted Average method, considering the

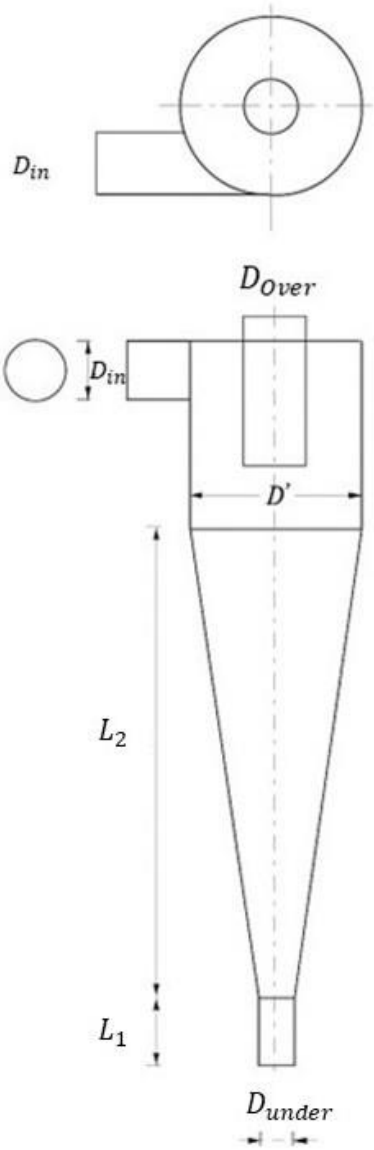

D_{in}/D	1/3
D_{under}/D	0.16
D_{over}/D	1/3
L_1/D	1/3
L_2/D	2.48
L_3/D	1/3
L_4/D	2/3

Fig. 2. Designed dimensions of hydrocyclone

Rys. 2. Wymiary projektowe hydrocyklonu

number of cells. It is noticed that this value does not suffer a notable change at 3,160,000 cells and beyond. The number of cells was chosen according to this criterion, as in Figure 4.

The current modeling involves a multiphase flow, with water as the continuous phase and inert oil droplets as the dispersed phase. A set of droplets will be injected, and their path will be observed from the moment of injection until their final fate. Where the multiphase flow exits

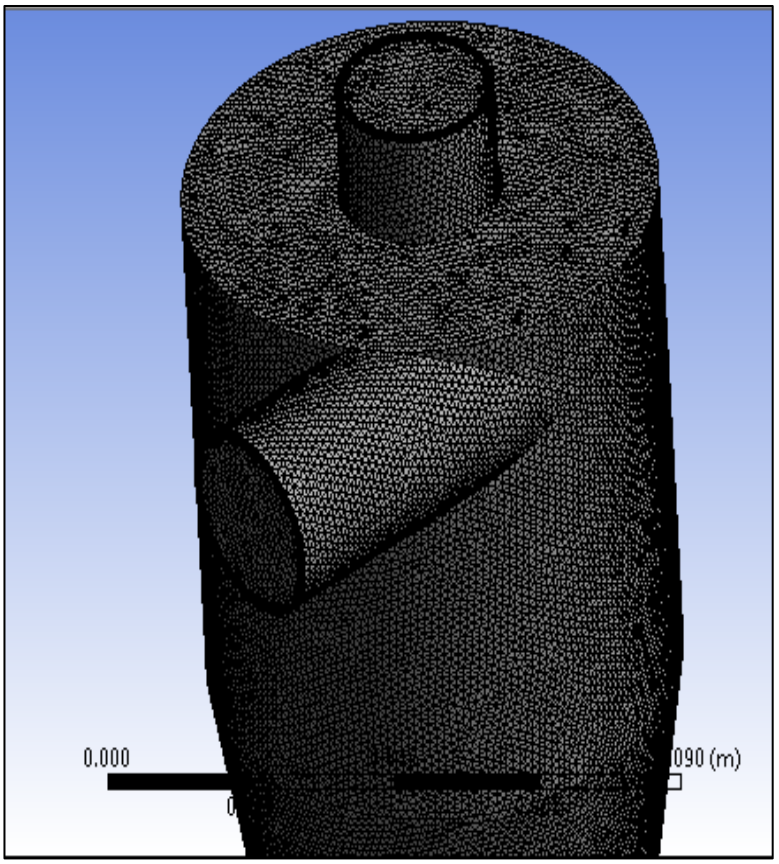

Fig. 3. Meshing of hydrocyclone

Rys. 3. Siatka hydrocyklonu

with the overflow and separates (as the low-density phase), or exits with the underflow, where the device fails to separate it. The basic properties of both phases include their density, as the working principle of this device is based on the difference in these densities. These properties are depicted in Table 2:

TABLE 2. Materials properties

TABELA 2. Właściwości materiałów

The quantity	Water	Oil
ρ [Kg/m^3]	998.2	890
μ [Pa·sec]	0.001003	0.00332

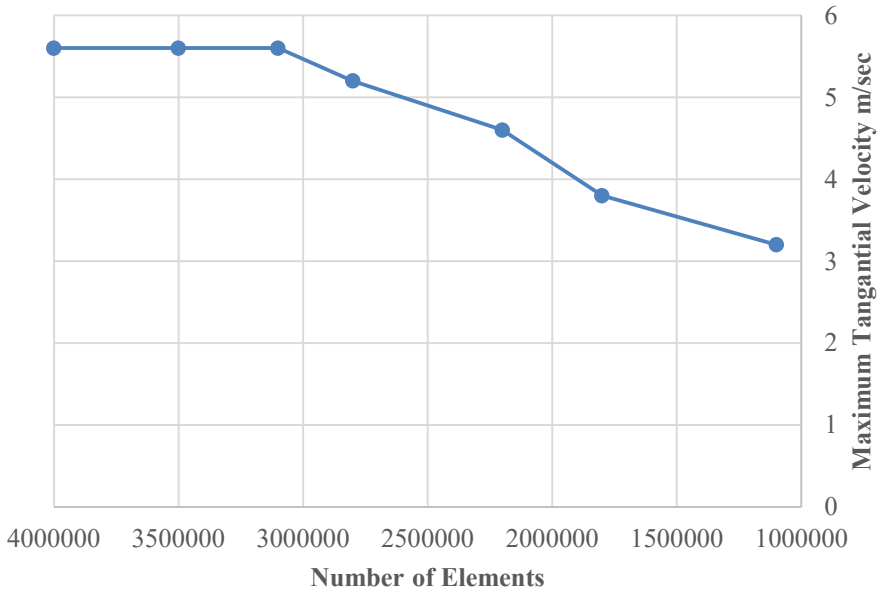

Fig. 4. Mesh independence study properties of materials used and boundary conditions

Rys. 4. Badanie niezależności siatki od właściwości stosowanych materiałów i warunków brzegowych

The basic boundary conditions used in this modeling are shown in Table 3:

Table 3. Boundary conditions

Tabela 3. Warunki brzegowe

Surface	Boundary condition type	Value
Inlet	velocity inlet	2.29 m/sec
Overflow	pressure outlet	zero-gauge pressure
Underflow	pressure outlet	zero-gauge pressure
Side wall	wall	no slip condition
Turbulence	intensity	5%
Turbulence	hydrolice diameter	0.025 m

1.5.2. Finite volume analysis and applied zones

The modeling will be performed using Ansys Fluent 16.1, with the Pressure-Based Solver in steady-state mode, and the gravitational constant set to a constant value of 9.81 m/s. The flow

modeling within the hydrocyclone is entirely a multiphase flow pattern. Figure 5 illustrates the simulation model, including the direction of flow at the inlet and outlet.

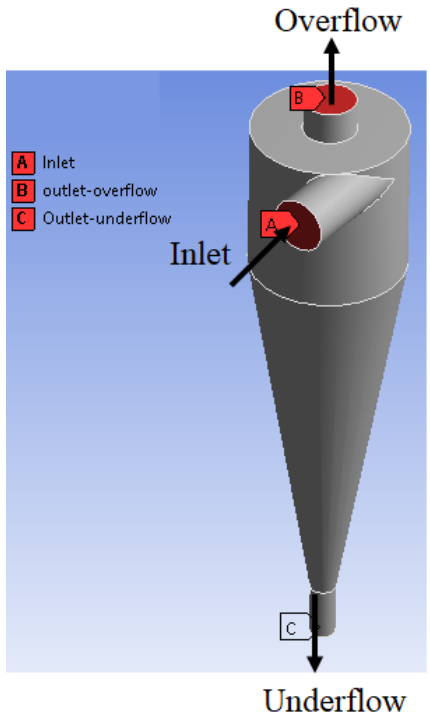

Fig. 5. The directions of flow in the hydrocyclone

Rys. 5. Kierunki przepływu w hydrocyklonie

2. Results

In this study, the modeling is divided into two stages according to the phases.

2.1. Stage 1 (continuous phase modeling)

At this stage, the flow field within the hydrocyclone for the aqueous phase, considered the continuous phase, is first determined by solving the conservation equations in the Eulerian reference frame using the RSM turbulence model. The velocity and pressure equations are

linked together, so the algorithm used to solve this link is the SIMPLE algorithm (Semi-Implicit Method for Pressure-Linked Equations), which achieves coupling between pressure and velocity in the continuity equations and momentum equations.

For the discretization of the equations, a second-order interpolation was used for each of the pressure, momentum, and kinetic energy of turbulence. Finally, to ensure the stability of the numerical solution, small under-relaxation factors between 0.3 and 0.5 were employed for each of the pressure, momentum, and turbulence energy equations. For the convergence of the solution, the residuals for each of the continuity equations, momentum, and Reynolds's stress components were set to a value of the order of 10^{-4}.

2.1.1. Continuous phase flow field results

The flow field is shown in the form of contour plots and graphs, where the contours are shown at the Z–Y plane corresponding to $X = 0$ and the graphs are drawn at the same plane at a height of ($Z = 0.226$ m) because experimental data are available at this height.

2.1.2. Tangential velocity

Figure 6 shows the tangential velocity contour, and the maximum tangential velocity can be determined to be approximately three times greater than the inlet velocity, which lies approximately at the boundary between the vortex-finder wall and the core of the hydrocyclone, in which an air core is likely to form. Cui et al. (2014) validated CFD velocity fields against PIV data in a 50 mm hydrocyclone, confirming combined vortex behavior and good agreement in axial and tangential velocities. Similarly, the current study reproduced velocity distributions with acceptable accuracy, in line with Cui et al. (2014) and Brennan (2006), who showed that RSM and LES can accurately predict tangential and axial velocity profiles when compared to Hsieh's experimental data. The present work achieved comparable accuracy using RSM, although LES (Brennan 2006) can further improve the prediction of fine-scale turbulence.

A positive value of the tangential velocity corresponds to a counterclockwise direction of rotation, and a negative value corresponds to a clockwise direction of rotation. It is essential to note that the direction of rotation in both the ascending and descending parts is the same. It follows the same direction of entry, except that this difference in direction is due to the high turbulence formed in the heart of the air core region, where small vortices are formed whose direction of rotation is clockwise, giving these negative values. Figure 7 shows the tangential velocity diagram, and Figure 8 compares this velocity at the mentioned location with the experimental results obtained from the reference study.

From Figure 8, the turbulence pattern used agrees very well with the experimental velocity values from the cyclone wall to the vortex wall, as mentioned (Bagheini 2014), and it predicts the location of the maximum velocity (where the vortex changes from free to forced). However,

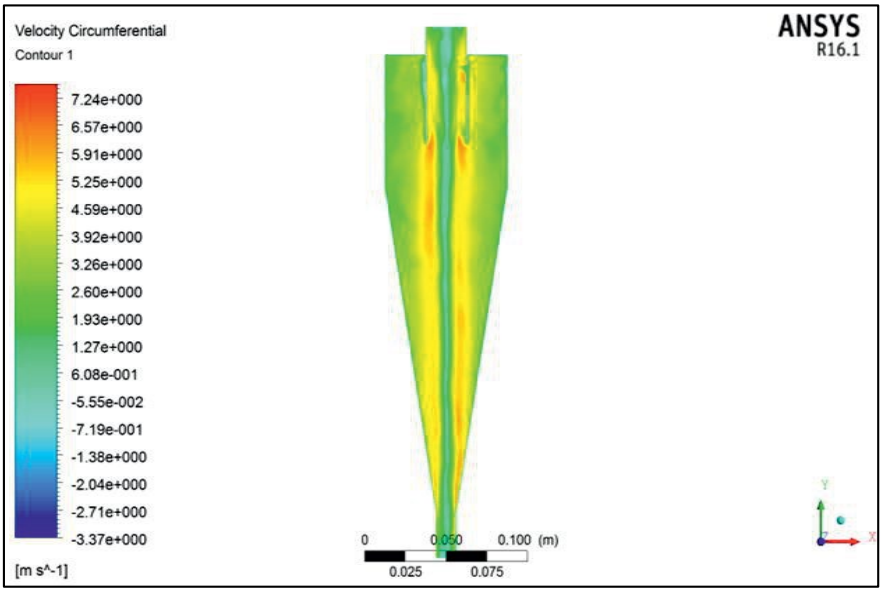

Fig. 6. Tangential velocity contours

Rys. 6. Kontury prędkości stycznej

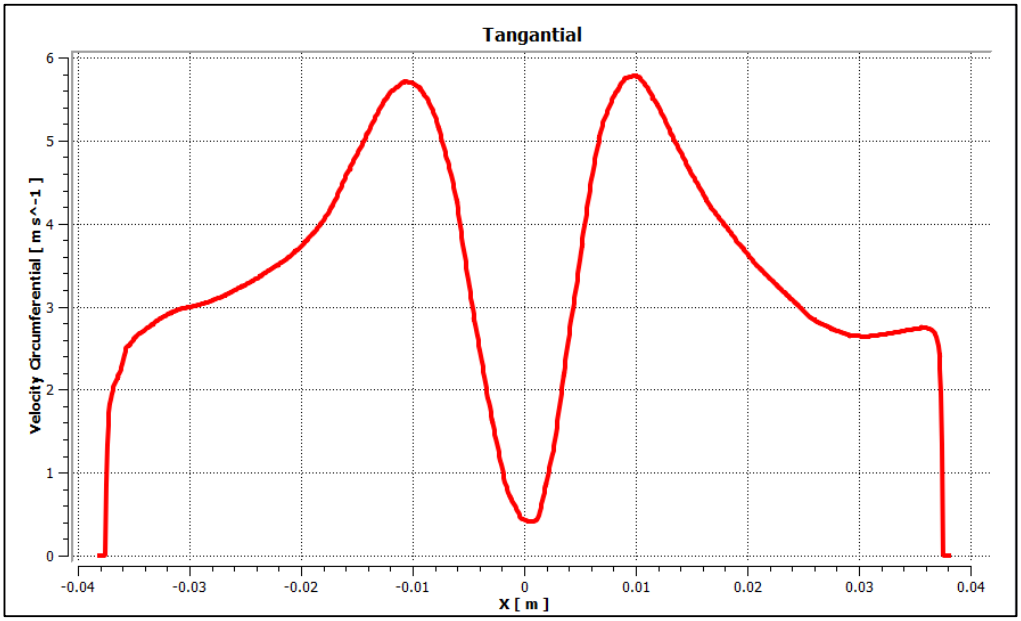

Fig. 7. Tangential velocity diagram

Rys. 7. Wykres prędkości stycznej

it does not specify this value with the required accuracy. In general, these results are acceptable to us because they give the correct shape of the flow pattern within the hydrocyclone.

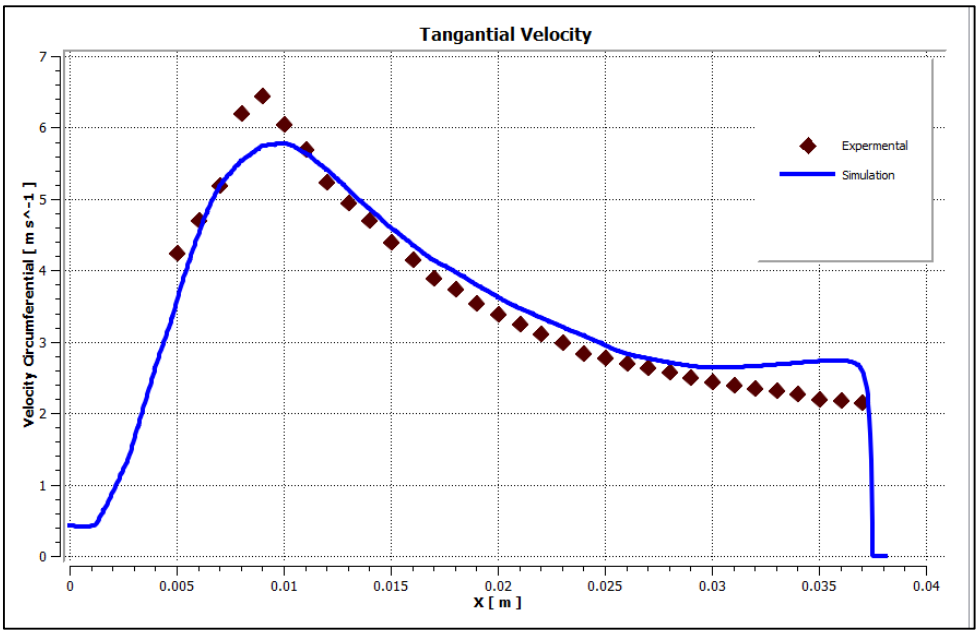

Fig. 8. Comparison between numerical and experimental tangential velocity

Rys. 8. Porównanie prędkości stycznej obliczonej metodą numeryczną i zmierzonej eksperymentalnie

2.1.3. Axial velocity

Figure 9 shows the axial velocity contour. It is noticed that there is a negative part representing downward flow and a positive part representing upward flow, with the maximum value of the axial velocity occurring in the upward part. For hydrocyclones used to separate liquids from solids with a higher density than the liquid, the downward part in the blue balloon is the place where they are located and will exit from the lower opening with the downward flow, while for hydrocyclones used to separate liquids from liquids (oil droplets with a lower density), the dark green field is the preferred place for them to be located and will exit with the upward flow.

Between these two fields (light green), the flow transitions from descending to ascending, which corresponds to the region where the axial velocity is zero, and the mantle is formed. As a result, there is a possibility of vortices forming in this area, which reduces the separation efficiency by distancing the light liquid from the ascending flow and increasing the likelihood of oil droplets breaking up into smaller droplets due to eddy currents. Figure 10 shows the axial velocity diagram, and Figure 11 compares this velocity at the mentioned location with the experimental results obtained from the reference study:

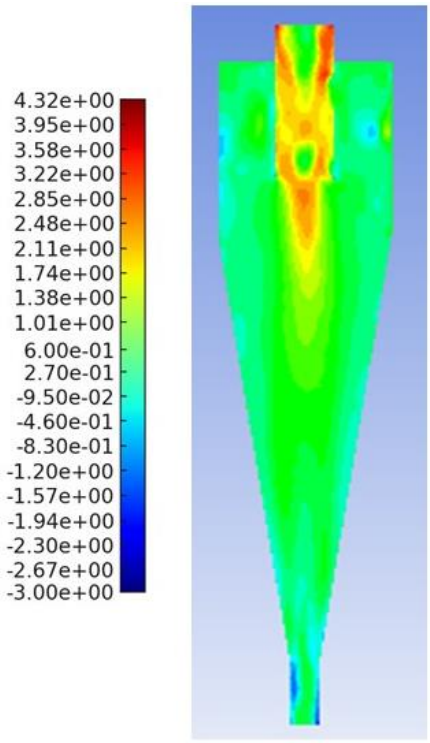

Fig. 9. Axial velocity contours

Rys. 9. Kontury prędkości osiowej

The modeling employed in this work demonstrates the accuracy of the results obtained by the modeling in comparison to the experimental results, as mentioned (Bagheini 2014), as the modeling accurately predicts the locations of the descending and ascending parts and provides an accurate value for the area and position of the reversal where the axial velocity is zero. Thus, it accurately predicts the location of mantle formation, and a slight deviation in the values of these velocities is observed. Comparing these two velocities with the experimental results yields an acceptable impression of the modeling, and this is an appropriate procedure for verifying the validity of the modeling in this study.

2.1.4. Total and static pressure

Figure 12 shows the total pressure contour in Pa.

A sky-blue region is depicted, representing a region of very low pressure, and is entirely compatible with the formation of an air or vapor core. The further movement away from the

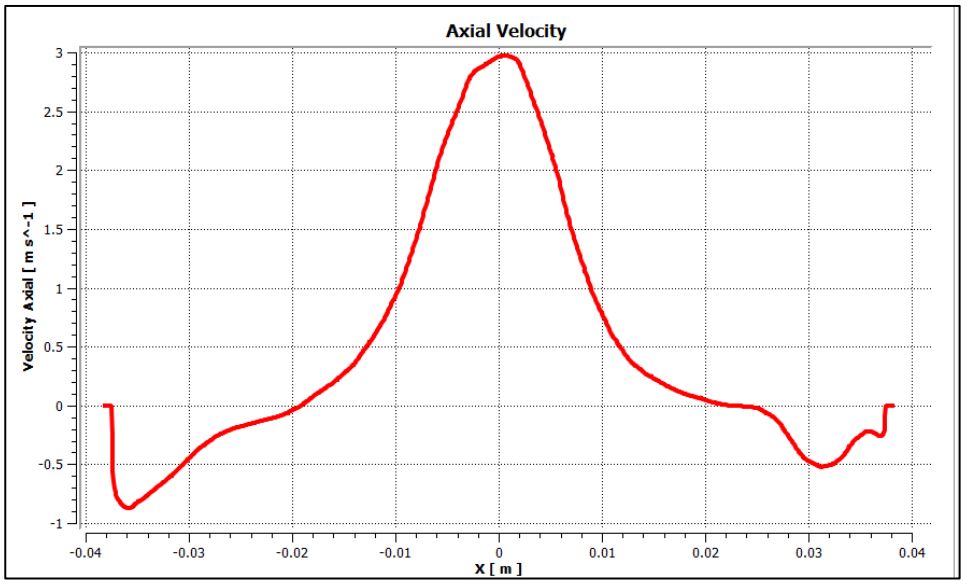

Fig. 10. Axial velocity diagram

Rys. 10. Wykres prędkości osiowej

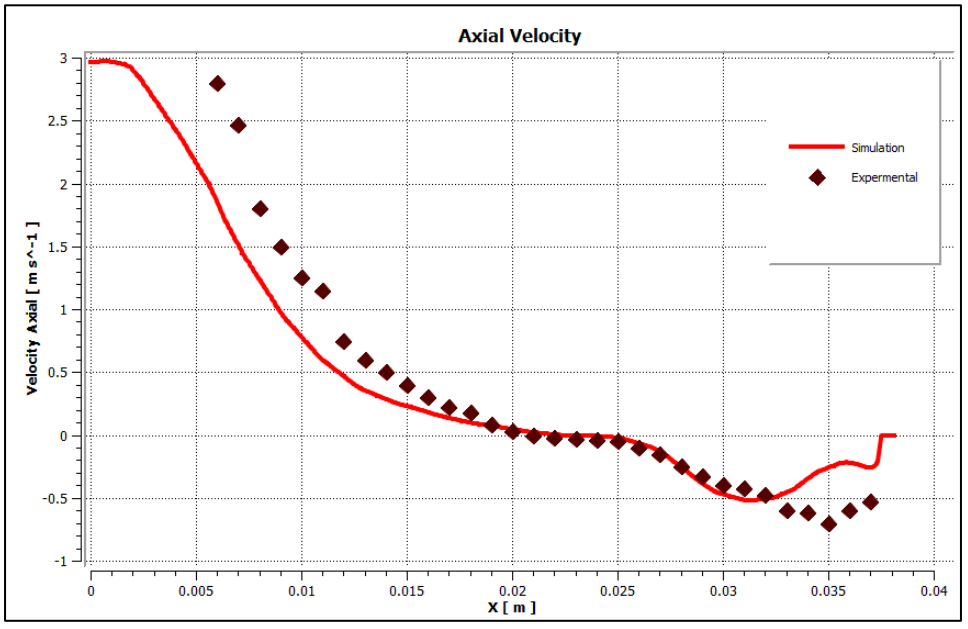

Fig. 11. Comparison between numerical and experimental axial velocity

Rys. 11. Porównanie prędkości osiowej obliczonej metodą numeryczną i zmierzonej eksperymentalnie

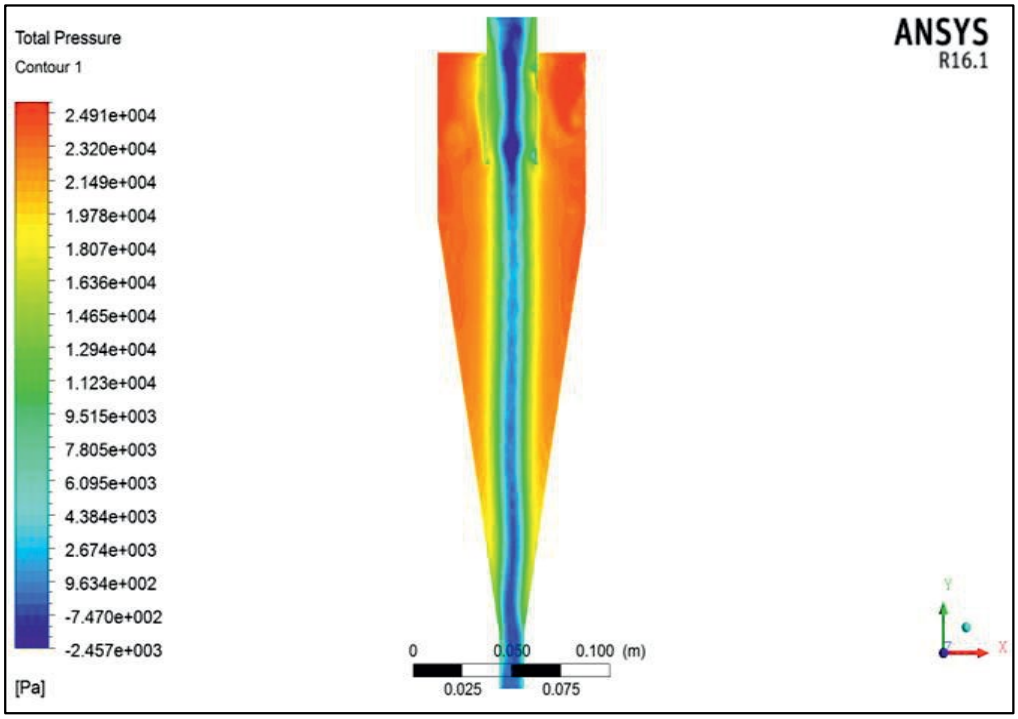

Fig. 12. Total pressure contours

Rys. 12. Kontury ciśnienia całkowitego

wall, the pressure increases, reaching its highest value at the wall, which is a fiery red. The difference between static pressure and total pressure represents the amount of dynamic pressure, and Figure 13 shows these diagrams, where red is static and black is total.

The negative component of static pressure is responsible for the formation of the air core. The numerical results confirm the reliability of the RSM turbulence model for capturing vortical structures.

2.2. Stage 2 (dispersed phase tracking)

At this stage, a set of diameters representing oil droplets will be injected, which will be tracked and traced by integrating their equation of motion within the Lagrangian reference system and knowing their final fate using the DPM (Discrete Phase Model) model in the steady state since the concentration of the dispersed phase is less than 10% in this application (purification for environmental purposes). A set of diameters (1 um, 5 um, 10 um, 25 um, 50 um, 75 um,

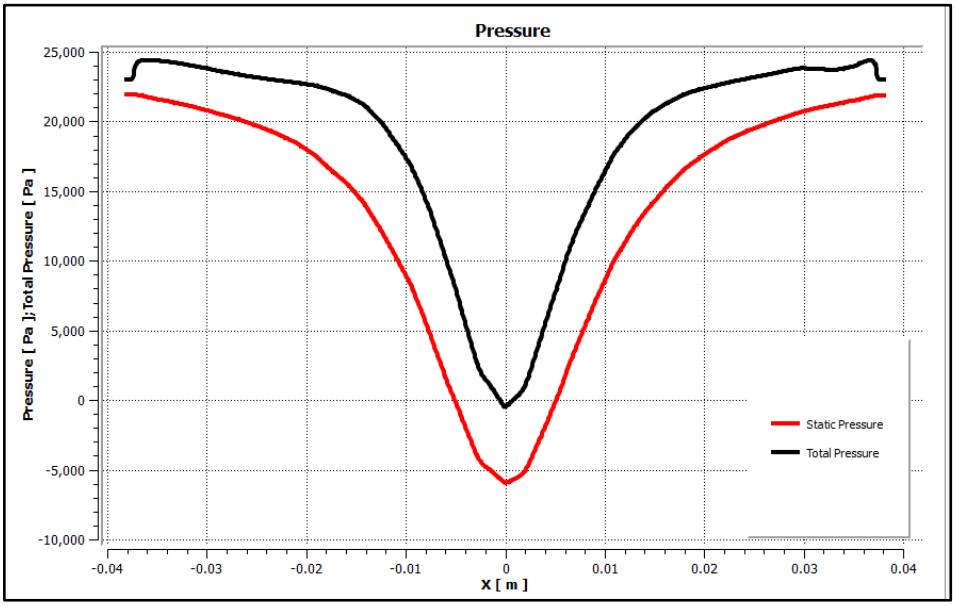

Fig. 13. Total and static pressure

Rys. 13. Ciśnienie całkowite i statyczne

100 um) is injected, and then track each particle and know its final fate. Figure 14 shows the fate of tracking several particles. Figure 15 shows the tracking of individual particles and their fate.

Cui et al. (2014) demonstrated that cone angle and overflow diameter strongly affect flow fields, while underflow diameter had little effect on velocities. The present study similarly identified design limitations, with unwanted water discharge in the overflow, suggesting that modifications to the vortex finder or underflow geometry could improve efficiency. Azimian and Bart (2016) additionally highlighted the impact of particle properties and erosion effects, pointing toward further considerations for long-term offshore applications.

By following some paths, the escaping droplets that were not separated by the ascending flow entered the descending flow through a lower opening at a large angle, thus reducing the distance traveled. Its residence time is reduced, and therefore, the separation efficiency is reduced, as the longer the particle remains within the device, the greater the separation efficiency. On the other hand, the droplets, separated by the ascending flow due to their low density compared to the continuous liquid phase, prefer to rotate with a smaller diameter and are dragged into the heart of the device, exiting with the ascending flow.

It is worth noting a very important point, which is that the principle of separation for liquids with liquids differs slightly compared to liquids and solids, as in the latter the density of solid particles is much higher compared to the continuous phase and therefore they will rotate at a larger diameter due to the centrifugal acceleration of the diameter to collide with the wall of the device and the forces of gravity will take care of dropping them to the downward flow

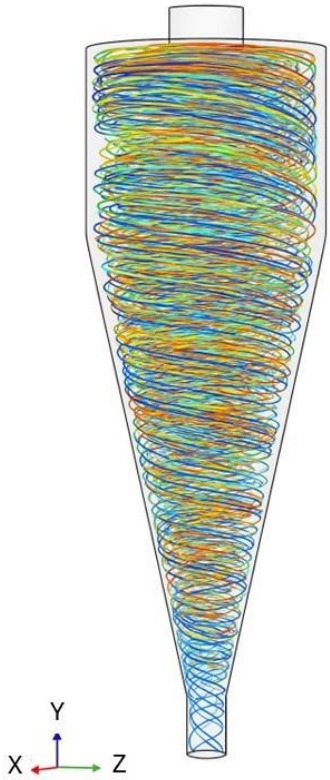

Fig. 14. The fate of tracking several particles

Rys. 14. Śledzenie kilku cząstek

and separate from the lower part and the larger the diameter the greater the centrifugal forces and therefore, the separation efficiency is greater, while in the first case the centrifugal forces affecting the droplets of the liquid with the lower density are smaller and therefore these droplets rotate at a smaller diameter for the buoyancy forces resulting from pressure to play the main role in the separation process and consequently the larger the droplets are the greater the buoyancy forces affecting them and therefore the separation efficiency increases. Figure 16 represents the distribution diagrams of the separation efficiency of these diameters:

The separation efficiency ranges from 80% for small droplets to 90% for large droplets, with a total separation yield of approximately 90%. This aligns with Medronho et al. (2005), who reported efficiencies approaching 90% for mammalian cell separation, and Azimian and Bart (2016), who validated CFD predictions of efficiency against experimental results for liquid-solid flows. The agreement across liquid–liquid and liquid–solid systems reinforces the robustness of CFD for hydrocyclone performance prediction.

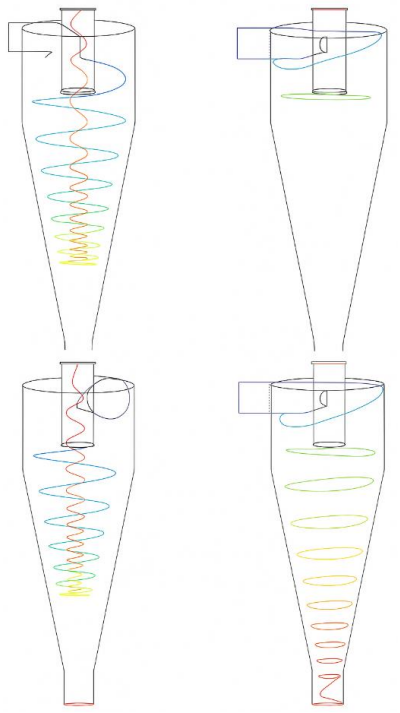

Fig. 15. The tracking of individual particles

Rys. 15. Śledzenie poszczególnych cząstek

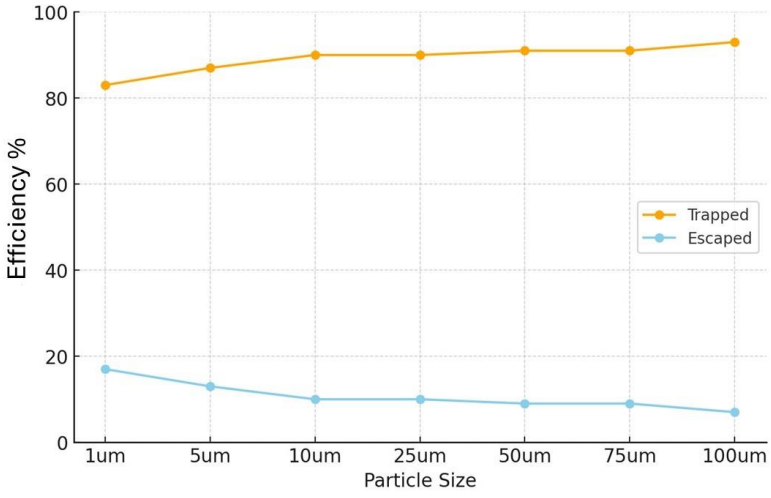

Fig. 16. The distribution diagrams of the separation efficiency

Rys. 16. Wykresy rozkładu wydajności separacji

2.3. Economic and environmental impact

In consideration of operational losses and environmental concerns, a comprehensive economic assessment was undertaken, and the results demonstrated that even minor percentages of water carryover exerted cumulative impacts on large-scale offshore operations, where daily throughput reached magnitudes of several thousand cubic meters. Figure 17 shows that both treatment cost and environmental risk increase linearly with water entrainment. Even at 2% water loss, the environmental impact is = 3.5 MUSD/year, while at 10% loss it can reach = 17.5 MUSD/year, compared to = 0.53 MUSD/year in treatment costs. This highlights that even small increases in overflow water loss have disproportionately large environmental consequences, underlining the importance of minimizing entrainment for both economic and regulatory reasons.

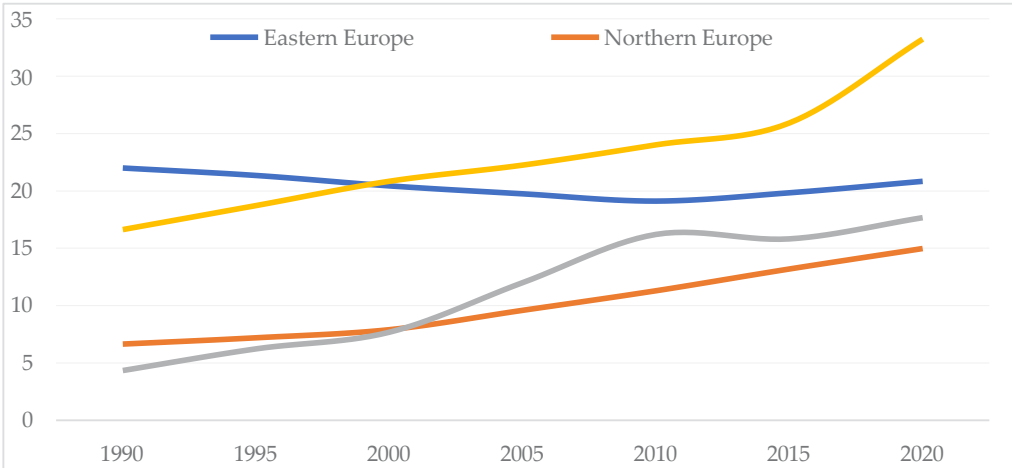

Fig. 17. Economic and environmental impact of water loss in hydrocyclone overflow

Rys. 17. Skutki gospodarcze i środowiskowe związane z utratą wody w przelewie hydrocyklonu

Conclusion

This study numerically modeled the separation of oil residues from produced water using a hydrocyclone with the Hsieh design, employing ANSYS Fluent 16.1. The continuous water phase was simulated with the Reynolds Stress turbulence model, while oil droplets were tracked through a Lagrangian approach with one-way coupling. The numerical predictions showed strong agreement with experimental reference data, validating the reliability of the adopted modeling approach. Flow field analysis successfully reproduced the tangential and

axial velocity profiles as well as the pressure distribution, including the formation of the air core. Particle tracking confirmed high performance, with separation efficiencies ranging from about 80% for small droplets to nearly 90% for larger droplets, yielding an overall efficiency close to 90%.

Nevertheless, mass flow analysis indicated that a portion of water was discharged with the overflow stream, highlighting a design limitation. This issue can potentially be resolved by modifying structural parameters such as the vortex finder or underflow diameter, or by optimizing operating conditions such as inlet velocity and pressure. From an industrial perspective, the demonstrated efficiency of 80–90% not only aligns with recent literature but also underscores the hydrocyclone's advantage as a cost-effective, low-maintenance, and energy-efficient separation technology. When coupled with design refinements to reduce water entrainment, hydrocyclones present a highly practical solution for large-scale offshore operations, balancing economic savings with environmental compliance.

Future research should focus on assessing alternative hydrocyclone geometries, applying advanced turbulence models for multiphase flow, and investigating transient operating conditions. Experimental validation under real offshore conditions and the integration of optimization algorithms for geometry and operating parameters are also recommended. Such developments would advance the practical application of hydrocyclones and further enhance oil-water separation efficiency in offshore installations.

The Authors have no conflicts of interest to declare.

References

Ali et al. 2023 – Ali, H.H.M., Hussein, A.M., Allami, K.M.H. and Mohamad, B. 2023. Evaluation of shell and tube heat exchanger performance by using ZnO/water nanofluids. *Journal of Harbin Institute of Technology* (New Series), 30, pp. 1–13, https://doi.org/10.11916/j.issn.1005-9113.2023001.

Ali et al. 2024 – Ali, H.H.M., Mohammed, A.J., Alshukri, M.J., Hussien, A.M. and Alsabery, A.I. 2024. Numerical study on entropy minimization in pipes with helical airfoil and CuO nanoparticle integration. *Open Engineering* 14(1), https://doi.org/10.1515/eng-2022-0594.

Amini et al. 2012 – Amini, S., Mowla, D., Golkar, M. and Esmaeilzadeh, F. 2012. Mathematical modelling of a hydrocyclone for the down-hole oil–water separation (DOWS). *Chemical Engineering Research and Design* 90(12), pp. 2186–2195, https://doi.org/10.1016/j.cherd.2012.05.007.

Azimian, M. and Bart, H.J. 2016. Numerical analysis of hydroabrasion in a hydrocyclone. *Petroleum Science* 13(2), pp. 304–319, https://doi.org/10.1007/s12182-016-0084-7.

Bagheini, S.G. 2014. *Basic Principles of Oil-water Separation by Hydrocyclone.* Doctoral thesis, University of Louisiana at Lafayette.

Barrak et al. 2022 – Barrak, A.S., Ali, N.M. and Ali, H.H.M. 2022. An effect of binary fluid on the thermal performance of pulsation heat pipe. *International Journal of Applied Mechanics and Engineering* 27(1), pp. 21–34, https://doi.org/10.2478/ijame-2022-0002.

Brennan, M. 2006. CFD simulations of hydrocyclones with an air core: Comparison between large eddy simulations and a second moment closure. *Chemical Engineering Research and Design* 84(6), pp. 495–505, https://doi.org/10.1205/cherd.05111.

Hsu et al. 2011 – Hsu, C-Y., Wu, S-J. and Wu, R-M. 2011. Particles Separation and Tracks in a Hydrocyclone. *Tamkang Journal of Science and Engineering* 14(1), pp. 65–70, https://doi.org/10.6180/jase.2011.14.1.08.

Collins, A.R. 2016. *Classification of multi-component feeds in a hydrocyclone*. Doctoral thesis, University of Queensland, Australia.

Cui et al. 2014 – Cui, B., Wei, D., Gao, S., Liu, W. and Feng, Y. 2014. Numerical and experimental studies of flow field in hydrocyclone with air core. *Transactions of Nonferrous Metals Society of China* 24(8), pp. 2642–2649, https://doi.org/10.1016/S1003-6326(14)63394-X.

Craik, A.D.D. 2013. Continuity and change: representing mass conservation in fluid mechanics. *Archive for History of Exact Sciences* 67(1), pp. 43–80, https://doi.org/10.1007/s00407-012-0108-7.

Delgadillo, J.A. and Rajamani, R.K. 2005. A comparative study of three turbulence-closure models for the hydrocyclone problem. *International Journal of Mineral Processing* 77(4), pp. 217–230, https://doi.org/10.1016/j.minpro.2005.06.007.

Ghodrat, M. 2014. *Computational modelling and analysis of the flow and performance in hydrocyclones.* Doctoral thesis, UNSW Sydney, https://doi.org/10.26190/unsworks/17028.

Hall, M. 1961. A theory for the core of a leading-edge vortex. *Journal of Fluid Mechanics* 11(2), pp. 209–228, https://doi.org/10.1017/S0022112061000470.

Karimi et al. 2012 – Karimi, M., Akdogan, G., Bradshaw, S.M. and Mainza, A. 2012. Numerical modelling of air core in hydrocyclones. [In:] *Ninth International Conference on CFD in the Minerals and Process Industries*, CSIRO, Melbourne, Australia.

Liu et al. 2015 – Liu, Y., Cheng, Q., Zhang, B. and Tian, F. 2015. Three-phase hydrocyclone separator – A review. *Chemical Engineering Research and Design* 100, pp. 554–560, https://doi.org/10.1016/j.cherd.2015.04.026.

Long et al. 2021 – Long, S., Lau, T.C., Chinnici, A. and Nathan, G.J. 2021. The flow-field within a vortex-based solar cavity receiver with an open aperture. *Experimental Thermal and Fluid Science* 123, https://doi.org/10.1016/j.expthermflusci.2020.110314.

Medronho et al. 2005 – Medronho, R.A., Schuetze, J. and Deckwer, W.-D. 2005. Numerical simulation of hydrocyclones for cell separation. *Latin American Applied Research* 35(1), pp. 1–8.

Motin, A. and Bénard, A. 2017. Design of liquid–liquid separation hydrocyclones using parabolic and hyperbolic swirl chambers for efficiency enhancement. *Chemical Engineering Research and Design* 122, pp. 184–197, https://doi.org/10.1016/j.cherd.2017.04.012.

Murthy, Y.R. and Bhaskar, K.U. 2012. Parametric CFD studies on hydrocyclone. *Powder Technology* 230, pp. 36–47, https://doi.org/10.1016/j.powtec.2012.06.048.

Németh, J. and Verdes, S. 2011. Flow pattern within hydrocyclone. *Hungarian Journal of Industry and Chemistry*, pp. 437–445, https://doi.org/10.1515/462.

Nowakowski, A.F. and Doby, M.J. 2008. The numerical modelling of the flow in hydrocyclones. *KONA Powder and Particle Journal* 26, pp. 66–80, https://doi.org/10.14356/kona.2008008.

Safa, R. and Goharrizi, A.S. 2014. CFD simulation of an industrial hydrocyclone with Eulerian–Eulerian approach: A case study. *International Journal of Mining Science and Technology* 24(5), pp. 643–648, https://doi.org/10.1016/j.ijmst.2014.07.010.

Sarpkaya, T. and Garrison, C.J. 1963. Vortex formation and resistance in unsteady flow. *Journal of Applied Mechanics* 30(1), pp. 16–24, https://doi.org/10.1115/1.3630099.

Sorsamäki, L. and Nappa, M. 2015. *Design and selection of separation processes*. VTT Technical Research Centre of Finland. VTT Research Report Vol. VTT-R-06143-15. [Online:] https://publications.vtt.fi/julkaisut/muut/2015/VTT-R-06143-15.pdf [Accessed: 2026-01-15].

Szwarc et al. 2025 – Szwarc, T., Wróblewski, W. and Borzęcki, T. 2025. Experimental and numerical study of the impact of the oil tank filling level on the aircraft separator. *FME Transactions* 50(1), pp.17–31. https://doi.org/10.22190/FUME211214016S.

Temam, R. 2001. *Navier–Stokes equations: theory and numerical analysis* (Vol. 343). American Mathematical Society.

Thiemsakul et al. 2024 – Thiemsakul, D., Piemjaiswang, R., Sema, T., Feng, Y., Piumsomboon, P. and Chalermsinsuwan, B. 2024. Effect of hydrocyclone design in microplastics-water separation by using computational fluid dynamics simulations. *Results in Engineering* 22, https://doi.org/10.1016/j.rineng.2024.102034.

Varaksin, A.Y. and Ryzhkov, S.V. 2022, Vortex flows with particles and droplets (A Review). *Symmetry* 14(10), https://doi.org/10.3390/sym14102016.

Xu et al. 2013 – Xu, H., Chen, X.H. and Yao, Y. 2013. Hydrocyclone velocity flow simulation and experimental study based on fluid mechanics. *Advanced Materials Research* 625, pp. 113–116, https://doi.org/10.4028/www.scientific.net/AMR.625.113.

Mustafa Naozad Taifor, Ali Azeez Ali, Furqan Haider Mohammed Ali, Adnan M. Hussein, Hussein Hayder Mohammed Ali, Mohammed Yashar Omar

Numeryczne modelowanie hydrocyklonu do separacji pozostałości olejowych w instalacjach morskich

Streszczenie

W niniejszym badaniu przeprowadzono numeryczną analizę procesu separacji oleju od wody w hydrocyklonie o konstrukcji Hsieha, wybranym ze względu na łatwość wykonania oraz sprawdzoną bazę danych eksperymentalnych. Symulacje dynamiki płynów (CFD) przeprowadzono w programie ANSYS Fluent 16.1 z wykorzystaniem modelu Eulera-Lagrange'a, w którym faza wodna została rozwiązana za pomocą modelu naprężeń Reynoldsa (RSM), a krople oleju śledzono za pomocą modelu fazy dyskretnej (DPM) w ramach sprzężenia jednokierunkowego. Badanie niezależności siatki potwierdziło stabilność rozwiązania przy 3,16 mln komórek, a zbieżność resztkowa została osiągnięta po około 1600 iteracjach, zapewniając dokładne prognozy prędkości, ciśnienia i tworzenia się rdzenia powietrznego. Wyniki numeryczne z powodzeniem odtworzyły charakterystyczny przepływ z podwójnym wiriem, odwrócenie prędkości osiowej oraz obszar ujemnego ciśnienia statycznego odpowiedzialny za rozwój rdzenia powietrznego, wykazując silną zgodność z opublikowanymi danymi eksperymentalnymi. Śledzenie cząstek wykazało, że wydajność separacji silnie zależy od wielkości kropelek, wzrastając z około 80% dla drobnych kropelek (1–5 µm) do maksymalnie prawie 90% dla większych kropelek (≥75 µm), co daje ogólną wydajność bliską 90%. Jednak część wody została porwana w przepływie przelewowym, ujawniając ograniczenia konstruk-

cyjne, które można złagodzić poprzez modyfikację geometrii wzniesienia wirowego lub przepływu podwirowego. Zweryfikowany model stanowi solidną podstawę do optymalizacji geometrii hydrocyklonów i warunków ich pracy, przyczyniając się do zwiększenia wydajności separacji ropy od wody, zmniejszenia ilości odprowadzanej wody oraz poprawy zgodności z przepisami środowiskowymi w morskich systemach wydobywczych.

Słowa kluczowe: separator hydrocyklonowy, separacja oleju od wody, model naprężeń Reynoldsa (RSM), model Hsieha, sedymentacja odśrodkowa